ENHANCED KNOWLEDGE IN SCIENCES AND TECHNOLOGY
e-ISSN: 2773-6385

EKST

Vol. 4 No. 2 (2024) 16-26
https://publisher.uthm.edu.my/periodicals/index.php/ekst

Hybrid Nanofluid Flow Over a Permeable Shrinking Cylinder with Magnetic Field

Nur Syazwani Mat Yusof[1], Fazlina Aman[1]*

[1] *Department of Mathematics and Statistics, Faculty of Applied Sciences and Technology, UTHM Kampus Cawangan Pagoh, Hab Pendidikan Tinggi Pagoh, KM 1, Jalan Panchor, 84600 Pagoh, Muar, Johor, MALAYSIA*

**Corresponding Author: fazlina@uthm.edu.my*
DOI: https://doi.org/10.30880/ekst.2024.04.02.003

Article Info

Received: 27 December 2023
Accepted: 11 January 2024
Available online: 12 December 2024

Keywords

Hybrid Nanofluid, Shrinking Cylinder, Shooting Technique, Runge-Kutta-Fehlberg Method, Heat Transfer, Magnetic Field

Abstract

This study explores the flow and heat transfer characteristics of Cu-Al_2O_3/water hybrid nanofluid over a permeable shrinking cylinder with magnetic field using the shooting technique. The research employs the Runge-Kutta-Fehlberg (RKF45) method in Maple to provide numerical solutions for the governing nonlinear partial differential equations. In the validation phase, the outcomes are compared with both an exact analytical solution and numerical values across various cases. Results indicate that the heat transfer rate varies with alumina and copper volumetric concentrations, with the least alumina concentration yielding the highest rate. The addition of alumina and copper volumetric concentration reduces the heat transfer rate. Temperature profile correlates positively with curvature parameter and Eckert number but inversely with the magnetic parameter. Velocity profile escalates with an increase in the magnetic parameter. This research contributes to understanding nanofluid heat transfer and provides a benchmark for future investigations into the influence of physical parameters and diverse hybrid materials.

1. Introduction

The application of hybrid nanofluid in addressing heat transfer challenges has emerged as a novel and promising approach. Engineers, researchers, and scientists are increasingly drawn to the extensive industrial, scientific, and technical applications of hybrid nanofluid, spanning microfluidics, generator cooling, transportation, manufacturing, medical lubrication, acoustics, naval structures, and solar heating. [1] introduced nanofluid, a substance formed by combining nanosized particles with a fluid, demonstrating exceptional potential for elevating thermal conductivity and heat transfer rates.

Nanofluids, composed of suspended nanoparticles ranging from 1 to 100 nanometers, modify the viscosity and thermal conductivity of the base fluid. Hybrid nanofluids, formed by combining nanoparticles of different types or with other additives, have been the subject of extensive study, particularly concerning their behavior under varying flow conditions. Early research by [2] experimented with hybrid nanoparticles, while subsequent studies by [3] and [4] explored the application of nanofluids for heat transfer enhancement. [5] investigated the potential of alumina hybrid nanoparticles to enhance fluid heat conduction. [6] conducted a comprehensive investigation into the Ellis hybrid nanofluid flow model, incorporating magnetic, Darcy-Forchheimer, and nonlinear thermal radiation effects on a stretching cylinder, revealing that increased Darcy-Forchheimer and magnetic parameters reduce the velocity profile of mono and hybrid nanofluids.

In addition to the nanofluid study, this research introduces a permeable shrinking cylinder, commonly found in biological systems and industrial applications. Such cylinders may undergo radial shrinkage while allowing fluid passage through their surfaces. [7] initiated the investigation of fluid flow over a stretching cylinder, with

[8] and [9] subsequently expanding on this work by considering effects like suction, injection, and velocity-slip. [10] explored the effects of a shrinking horizontal cylinder on the unsteady stagnation-point flow of a TiO2 C2H6O2 nanofluid, considering a magnetic field, joule-heating viscous dissipation, nanoparticle aggregation, and mass suction, revealing that increased unsteadiness, magnetic field, and nanoparticle volume fraction parameters elevate velocity and temperature profiles, while curvature and suction parameters exhibit an inverse relationship.

The idea of multiple shooting was first put forth by [11] and then advanced by [12], who created and examined both a simple shooting method (SSM) and a multiple shooting method (MSM). [13] applied a shooting technique based on RK-4 algorithms (bvp4c) to transform governed flow expressions partial differential equations (PDEs) into ordinary differential equations (ODEs) in their numerical investigation, revealing the flow characteristics of a hybrid nanomaterial (SWCNTs + CuO + Engine oil) over a curved stretched sheet with Darcy-Forchheimer porous medium. [14] explored the application of the Newton built-in shooting technique to solve non-dimensional systems, transforming given partial differential systems into dimensionless ordinary expressions for the analysis of Darcy-Forchheimer nanoliquid flow over a stretched surface. [15] innovatively introduced a versatile numerical tool, utilizing the shooting technique, to assess coefficient matrices of subdomains without prior knowledge of the semi-discretized system's analytical solution, demonstrating universal applicability and precision through comparisons with the closed-form solution of linear electrostatics while accommodating various direct solution approaches.

The impact of external fields on fluid dynamics holds paramount significance in numerous natural and industrial flow scenarios. One such influential external force is the magnetic field, giving rise to the field of magnetohydrodynamics. This branch of study focuses on analyzing the dynamics of electrically conductive fluids, including plasma and liquid metals [16–18]. Various approaches exist for modeling the effects induced by applied magnetic fields on current and energy fields. One approach involves the solution of the coupled Navier-Stokes and energy equations, while a more streamlined method incorporates volumetric forces such as the Lorenz or Kelvin forces directly into the momentum equations [19–21]. These methodologies offer diverse avenues for comprehending and simulating external magnetic fields and fluid behavior in a range of practical applications.

Inspired by previous literature, this study specifically investigates the Cu-Al2O3/water hybrid nanofluid, widely reported in the field. The choice of this nanofluid serves as an exemplary case for analysing the combined effects of copper and alumina nanoparticles. This research investigates heat transfer in a hybrid Cu-Al2O3/water nanofluid with least alumina concentration and explores how increasing the volume fraction of copper nanoparticles enhances heat transfer, maintaining a fixed 10% alumina fraction.

A key novelty lies in applying an effective solution method to analyse nanofluid flow over a permeable shrinking cylinder. Contrary to earlier research using MATLAB's bvp4c solver, our approach employs RKF45 with a shooting technique in MAPLE software, comparing results with [22]. The widely recognized RKF45 method, coupled with the shooting technique, holds significance in scientific research, providing a benchmark for validation. This method aids in understanding complex fluid dynamics, heat transfer, and nanoparticle transport in hybrid nanofluid systems.

This paper sheds light on the complexity of hybrid nanofluid behaviour in the context of MHD flow around a shrinking cylinder with the influence of Joule heating and addresses critical issues through various solution methods, paving the way for innovative technologies with broad implications.

2. Research Method

A steady, incompressible hybrid nanofluid with a magnetic field is studied on a permeable radially stretching or shrinking cylinder of radius a. As depicted in Fig. 1, the hybrid nanofluid is expected to flow along the axial x-direction with the r-coordinate being normal to x, and the r-axis is paralleled by a B_0 which is transverse magnetic field of strength that has zero electric field. The shrinking cylinder has a linear velocity $U_w(x)$ and a constant characteristic velocity u_0 such that $U_w(x) = u_0 x/L$. The constant mass flux velocity is denoted by $v_w(r)$ where $v_w(r) > 0$ refers to injection or fluid removal and $v_w(r) < 0$ represents suction.

Enhanced Knowledge in Sciences and Technology Vol. 4 No. 2 (2024) p. 16-26

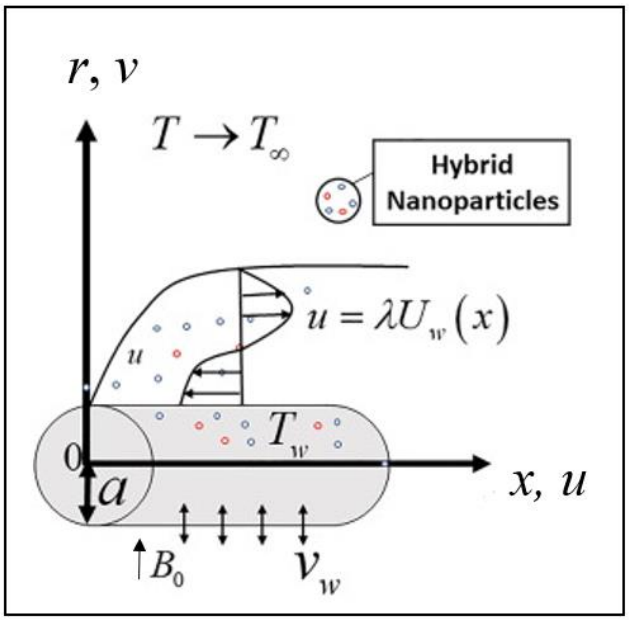

Fig. 1 Physical configuration and coordinate system ([22])

Following [23] single-phase nanofluid model and boundary layer assumptions, the governing equations of the hybrid nanofluid are:

$$\frac{\partial(ru)}{\partial x}+\frac{\partial(rv)}{\partial r}=0 \tag{1}$$

$$u\frac{\partial u}{\partial x}+v\frac{\partial u}{\partial r}=\frac{\mu_{hnf}}{\rho_{hnf}}\left(\frac{\partial^2 u}{dr^2}+\frac{1}{r}\frac{\partial u}{\partial r}\right)-\frac{\sigma_{hnf}B_0^2}{\rho_{hnf}}u, \tag{2}$$

$$u\frac{\partial T}{\partial x}+v\frac{\partial T}{\partial r}=\frac{k_{hnf}}{\left(\rho C_p\right)_{hnf}}\left(\frac{\partial^2 T}{\partial r^2}+\frac{1}{r}\frac{\partial T}{\partial r}\right)+\frac{\sigma_{hnf}B_0^2}{\left(\rho C_p\right)_{hnf}}u^2, \tag{3}$$

subject to the boundary conditions that can be expressed as:

$$v=v_w(r),\ u=\lambda U_w(x),\ T=T_w(x),\ \text{at } r=a,$$
$$u\to 0,\ T\to T_\infty,\ \text{as } r\to\infty, \tag{4}$$

where T is the temperature of the hybrid nanofluid, and u and v, respectively, stand in for the velocities along the x- and r-axes. The variable wall temperature is calculated as $T_w = T_\infty + T_0\,(x/L)^2$, where T_0 is the characteristic temperature, L is the characteristic length of the cylinder and the ambient hybrid nanofluid temperature T_∞ is constant. λ stands for the constant parameter of shrinking ($\lambda < 0$), and $\lambda = 0$ represents the static cylinder.

It is important to note that the first and second solid nanoparticles are denoted as $s1$ and $s2$, respectively, while the regular (base) fluid, hybrid, and traditional nanofluids are abbreviated as f, hnf, and nf, respectively. Here, dynamic viscosity μ_{hnf}, density ρ_{hnf}, heat capacitance $\left(\rho C_p\right)_{hnf}$, thermal conductivity k_{hnf}, and electrical conductivity σ_{hnf} are used in Eqs. (2) and (3).

2.1 Thermophysical properties

The thermophysical properties of single and hybrid nanofluids are shown in Table 1. In addition, Table 2 lists the thermophysical characteristics of the first nanoparticle (copper, Cu), second nanoparticle (alumina, Al_2O_3) and pure water.

Table 1 Thermophysical properties of single and hybrid nanofluids ([24-26])

Properties	Single Nanofluid	Hybrid Nanofluid
Density	$\rho_{nf} = \left(1-\phi_1\right)\rho_f + \phi_1\rho_{s1}$	$\rho_{hnf} = \left(1-\phi_2\right)\left[\left(1-\phi_1\right)\rho_f + \phi_1\rho_{s1}\right] + \phi_2\rho_{s2}$
Heat Capacity	$\left(\rho C_p\right)_{nf} = \left(1-\phi_1\right)\left(\rho C_p\right)_f + \phi_1\left(\rho C_p\right)_{s1}$	$\left(\rho C_p\right)_{hnf} = \left(1-\phi_2\right)\left[1-\phi_1\left(\rho C_p\right)_f + \phi_1\left(\rho C_p\right)_{s1}\right] + \phi_2\left(\rho C_p\right)_{s2}$
Dynamic Viscosity	$\frac{\mu_{nf}}{u_f} = \frac{1}{\left(1-\phi_1\right)^{2.5}}$	$\frac{\mu_{hnf}}{u_f} = \frac{1}{\left(1-\phi_1\right)^{2.5}\left(1-\phi_2\right)^{2.5}}$
Thermal Conductivity	$\frac{k_{nf}}{k_f} = \left[\frac{k_{s1}+2k_f-2\phi_1\left(k_f-k_{s1}\right)}{k_{s1}+2k_f+\phi_1\left(k_f-k_{s1}\right)}\right]$	$\frac{k_{hnf}}{k_{hf}} = \left[\frac{k_{s2}+2k_{hf}-2\phi_2\left(k_{hf}-k_{s2}\right)}{k_{s2}+2k_{hf}+\phi_2\left(k_{hf}-k_{s2}\right)}\right]$ where $\frac{k_{hf}}{k_f} = \left[\frac{k_{s1}+2k_f-2\phi_1\left(k_f-k_{s1}\right)}{k_{s1}+2k_f+\phi_1\left(k_f-k_{s1}\right)}\right]$
Electrical Conductivity	$\frac{\sigma_{nf}}{\sigma_f} = 1+\frac{3(\sigma-1)\phi_1}{2+\sigma-(\sigma-1)\phi_1}$ where $\sigma=\sigma_{s1}/\sigma_f$	$\frac{\sigma_{hnf}}{\sigma_{hf}} = \left[\frac{\sigma_{s2}+2\sigma_{hf}-2\phi_2\left(\sigma_{hf}-\sigma_{s2}\right)}{\sigma_{s2}+2\sigma_{hf}+\phi_2\left(\sigma_{hf}-\sigma_{s2}\right)}\right]$ where $\frac{\sigma_{hf}}{\sigma_f} = \left[\frac{\sigma_{s1}+2\sigma_f-2\phi_1\left(\sigma_f-\sigma_{s1}\right)}{\sigma_{s1}+2\sigma_f+\phi_1\left(\sigma_f-\sigma_{s1}\right)}\right]$

Table 2 Thermophysical properties of cuprum/copper, alumina/aluminium oxide, pure water ([24-26] and [27])

Physical properties	Cu	Al_2O_3	Water
$\rho\left(\mathrm{kg/m^3}\right)$	8933	3970	997.1
$C_p\left(\mathrm{J/kgK}\right)$	385	765	4179
$k\left(\mathrm{W/mK}\right)$	400	40	0.6130
$\sigma\left(\mathrm{s/m}\right)$	59.6×10^6	35×10^6	5.5×10^{-6}

For alumina and copper, respectively, the volumetric concentration of nanoparticles is ϕ_1 and ϕ_2. Here, ϕ is the nanoparticles volume fraction, ρ_s and ρ_f are the densities of the hybrid nanoparticles and base fluid, respectively, C_p is the heat capacity with constant pressure, $(\rho C_p)_s$ and $(\rho C_p)_f$ are the heat capacitances of the hybrid nanoparticles and base fluid, respectively, k_s *and* k_f are the thermal conductivities of the hybrid nanoparticles and base fluid, accordingly, and σ_s and σ_f are the electrical conductivities of the hybrid nanoparticles and base fluid, correspondingly. If $\phi_1 = \phi_2 = 0$, then hybrid nanofluid reduces to a viscous regular fluid.

2.2 Similarity transformation

The similarity transformation is used to convert the nonlinear PDEs of continuity equation (1), momentum equation (2), and energy equation (3) into ODEs. The similarity variables are as follows:

$$u = \frac{u_0 x}{L} f'(\eta),\ v = -\frac{a}{r}\sqrt{\frac{u_0 v_f}{L}} f'(\eta),\ \theta(\eta) = \frac{T-T_\infty}{T_w-T_\infty},$$

$$\eta = \sqrt{\frac{u_0}{v_f L}}\,\frac{r^2-a^2}{2a}, \tag{5}$$

so that

$$v_w(r) = -\frac{a}{r}\sqrt{\frac{u_0 v_f}{L}}S,$$

where S is the mass flux parameter, $S > 0$ for suction, $S < 0$ for injection, and primes signify differentiation with respect to η. To establish a connection with curvature, the variable η in the given equation plays a crucial role. The parameter a in the equation has the potential to influence curvature, necessitating a closer examination of the factors associated with a, specifically η. By considering fixing the value of L, while allowing a to vary, this is where the curvature changes. In this context, curvature refers to the variable η. It's important to note that r in the equation is a variable, signifying that the diameter undergoes alterations, creating an association with curvature. The variables in the equation, including r and a, play a pivotal role in describing how changes in diameter relate to alterations in curvature.

An addition, the continuity equation (1) is obeyed by the transformation in Eq. (5). Using the similarity transformations, the nonlinear partial equations (2) and (3) with boundary conditions (4) are reduced to the following nonlinear ODEs:

$$\frac{\mu_{hnf}/\mu_f}{\rho_{hnf}/\rho_f}\left[(1+2\gamma\eta)f'''(\eta)+2\gamma f''(\eta)\right]+ff''(\eta)-f'^2-\frac{\sigma_{hnf}/\sigma_f}{\rho_{hnf}/\rho_f}Mf'(\eta)=0, \tag{6}$$

$$\frac{1}{\Pr}\frac{k_{hnf}/k_f}{(\rho C_p)_{hnf}/(\rho C_p)_f}\left[(1+2\gamma\eta)\theta''(\eta)+2\gamma\theta'(\eta)\right]+f(\eta)\theta'(\eta)-2f'(\eta)\theta(\eta)$$
$$+\frac{\sigma_{hnf}/\sigma_f}{(\rho C_p)_{hnf}/(\rho C_p)_f}Ec\,M f'^2(\eta)=0, \tag{7}$$

with the boundary conditions

$$f(0)=S,\ f'(0)=\lambda,\ \theta(0)=1,$$
$$f'(\infty)\to 0,\quad \theta(\infty)\to 0, \tag{8}$$

Given,

$$\gamma=\sqrt{\frac{v_f L}{u_0 a^2}},\quad M=\frac{\sigma_f L B_0^2}{\rho_f u_0},\quad v_f=\frac{\mu_f}{\rho_f},$$

The physical quantities of interest are local skin friction coefficient and local Nusselt number which are defined as

$$C_f=\frac{\mu_{hnf}}{\rho_f U_w^2}\left(\frac{\partial u}{\partial r}\right)_{r=a},\quad Nu_x=\frac{x\,k_{hnf}}{k_f(T_w-T_\infty)}\left(-\frac{\partial T}{\partial r}\right)_{r=a},$$

Hence

$$Re_x^{1/2}C_f=\frac{f''(0)}{(1-\varphi_1)^{2.5}(1-\varphi_2)^{2.5}},\quad Re_x^{-1/2}Nu_x=-\frac{k_{hnf}}{k_f}\theta'(0), \tag{9}$$

3. Results and Discussion

The resulting of the similarity equations (6) and (7), subject to the boundary condition (8), is obtained using the shooting method with RKF45 algorithm implemented in Maple. The results are analyzed and presented in the form of tables (Tables 3, 4, and 5) and graphical representations (Figs. 2-6). The execution of the RKF45 method involves the selection of governing parameters, ensuring convergence by adjusting the boundary layer thick-

ness, η_∞. Throughout the process, fixed values of Pr = 6.2, alumina volumetric concentration ϕ_1= 0.1, and suction parameter *S* are maintained, while other physical parameters are systematically tested within defined ranges. Specifically, the shrinking region is explored with varying values such that $0 \leq \phi_2 \leq 0.02$, $0 \leq \gamma \leq 0.2$, $0.1 \leq M \leq 0.15$ and $0.01 \leq Ec \leq 1$.

Maple software helps generate important values successfully, including the skin friction coefficient, $f''(0)$ and the local Nusselt number, $\theta'(0)$. Notably, the chosen values for Prandtl number, Pr, mass transpiration parameter, *S*, shrinking parameter, λ, nanoparticle volume fractions for copper, ϕ_2, and the nanoparticle volume fraction for alumina, ϕ_1 align with those employed in the prior study conducted by [22].

Table 3 $Re_x^{1/2} C_f$ when S = γ = M = Ec = 0, Pr = 6.135, ϕ_1 = 0.1, λ =1 and various ϕ_2

ϕ_2	$Re_x^{1/2} C_f = \frac{\mu_{hnf}}{\mu_f} f''(0)$		
	[22]	Analytical [22]	Present Results
0.005	-1.327098	-1.327097962	-1.327097962
0.02	-1.409490	-1.40949019	-1.40949019
0.04	-1.520721	-1.520721211	-1.520721211
0.06	-1.634119	-1.634118687	-1.634118687

Table 4 $Re_x^{-1/2} Nu_x$ when S = γ = M = Ec = 0, Pr = 6.135, ϕ_1 = 0.1, λ =1 and various ϕ_2

ϕ_2	$Re_x^{-1/2} Nu_x = -\frac{k_{hnf}}{k_f}\theta'(0)$
0.005	1.961773
0.02	1.989308
0.04	2.026446
0.06	2.064150

In Table 3, it is observed that the skin friction coefficient becomes increasingly negative with a rise in ϕ_2 from 0.005 to 0.06. This negative trend signifies that, as ϕ_2 increases, there is a corresponding enhancement in skin friction. The introduction of additional nanoparticles into the flow results in reduced flow motion, concurrently thinning the momentum boundary layer. The present results also demonstrate good agreement with the previous study by [22].

Furthermore, the variation of the local Nusselt number, $Re_x^{-1/2} Nu_x$, for different values of ϕ_2 is explored under the conditions of $S = \gamma = M = Ec = 0$, Pr = 6.135, ϕ_1= 0.1, and λ = 1, as depicted in Table 4. This table is included for future reference, providing a comprehensive overview of the heat transfer characteristics under varied nanoparticle concentrations. It shows that with the presence of ϕ_2, the heat transfer rate at the surface increases significantly.

The influence of the curvature parameter on velocity profiles is clarified in Fig. 2, revealing its impact. It is important to note that a gradual increase in the curvature parameter corresponds to a proportional decrease in velocity profiles. Fig. 3 illustrates the impact of the magnetic parameter, *M* on velocity profiles, showing that an elevated *M* correlates with an enhanced velocity profile, highlight the significant role of the magnetic parameter in augmenting velocity within the hybrid nanofluid.

Enhanced Knowledge in Sciences and Technology Vol. 4 No. 2 (2024) p. 16-26

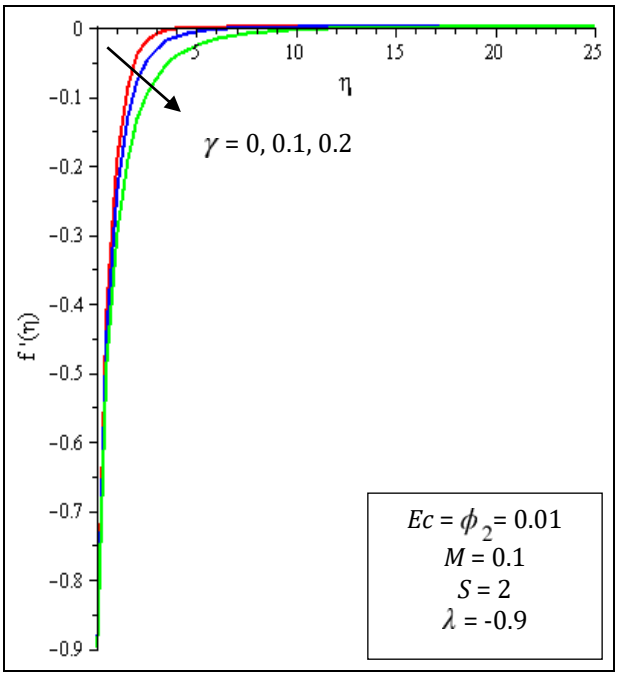

Fig. 2 Velocity profile against η for various γ

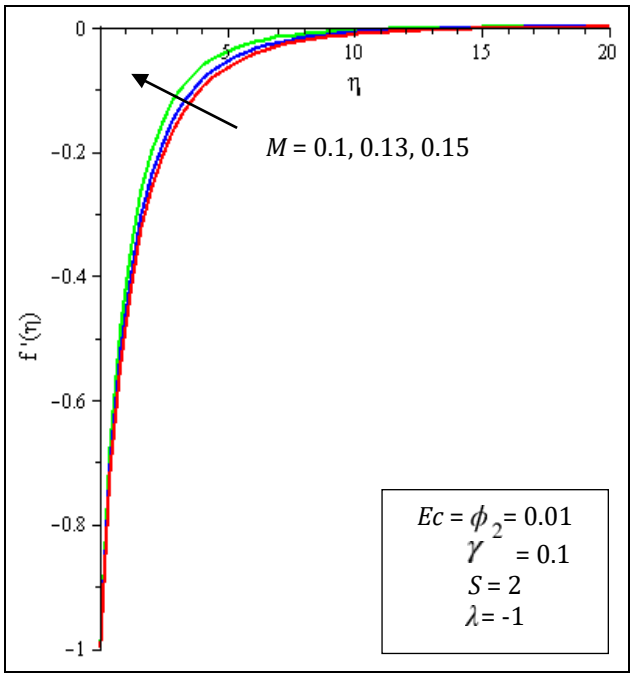

Fig. 3 Velocity profile against η for various M

Examining temperature profiles, $\theta(\eta)$ in Fig. 4, a rising trend concurrent with an increase in the curvature parameter. Moving on to Fig. 5, the results depict the influence of *Ec* on temperature profiles, where an increased *Ec* corresponds to a heightened temperature profile. Finally, Fig. 6 showcases the impact of the magnetic parameter on temperature profiles, indicating a noticeable decrease with higher magnetic parameter values, implying a reduction in the heat transfer rate at the surface of the hybrid nanofluid.

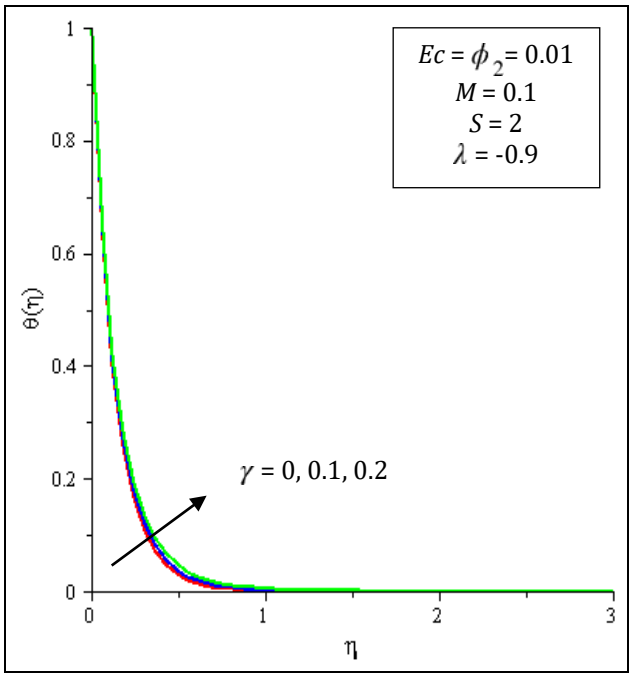

Fig. 4 Temperature profile against η for various γ

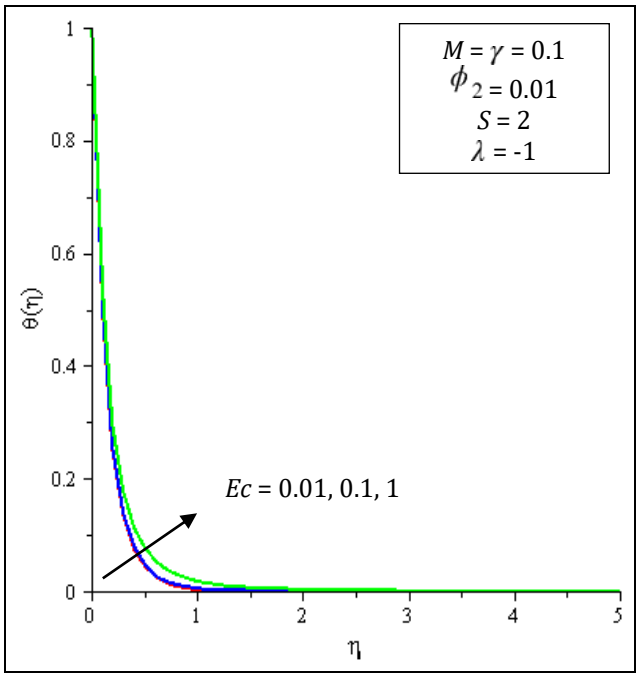

Fig. 5 Temperature profile against η for various Ec

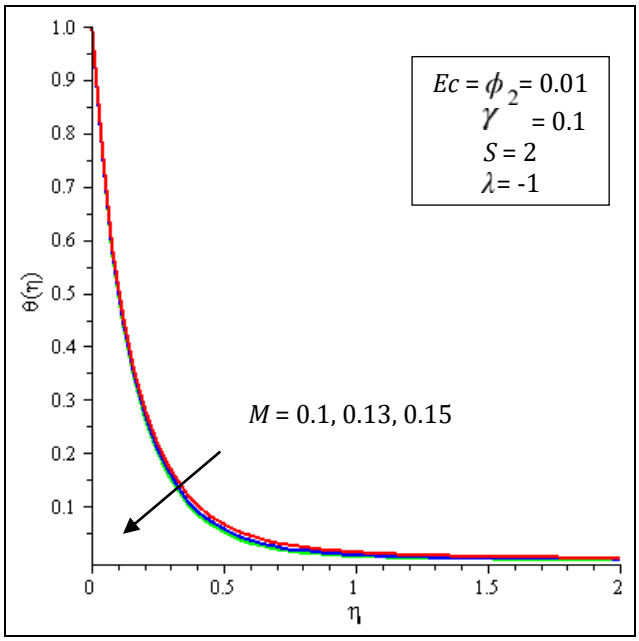

Fig. 6 Temperature profile against η for various M

Table 5 presents comprehensive data on the skin friction coefficient and local Nusselt number under specific conditions when η_∞ = 30, S = 2, M = 0.1, Ec = 0.01, Pr = 6.2, and λ = -1. The results are categorized by varying ϕ_1, ϕ_2, and γ.

Table 5 $Re_x^{1/2}C_f$ and $Re_x^{-1/2}Nu_x$ when η_∞ = 30, S = 2, Pr = 6.2, λ = -1, M = 0.1, and $Ec = 0.01$ with various ϕ_1, ϕ_2, and γ

γ	ϕ_1	ϕ_2	$Re_x^{1/2}C_f$		$Re_x^{-1/2}Nu_x$	
			Khashi'ie *et al.* [22]	Present results	Khashi'ie *et al.* [22]	Present results
0	0	0	1.31623	1.31622	10.81700	10.81699
	0.1	0	1.70970	1.70969	9.94958	9.94957
	0	0.02	1.64507	1.64506	10.72459	10.72458
	0.1	0.02	2.01134	2.01134	9.84403	9.84402
0.1	0.03	0.02	1.66224	1.66224	10.40085	10.40083
	0.05	0.02	1.72939	1.72939	10.21611	10.21609
	0.1	0.02	1.85323	1.85322	9.69708	9.69707
		0.01	1.65783	1.65782	9.73266	9.73265

Notably, the skin friction coefficient and local Nusselt number for a hybrid nanofluid with ϕ_1 = 0.1 and ϕ_2 = 0.02 are observed to be higher on a flat plate (γ = 0) compared to a cylinder with 10% curvature (γ = 0.1).

Furthermore, under specific conditions (γ = 0.1 and ϕ_2 = 0.02), an increase in ϕ_1 leads to an increment in the skin friction coefficient, causing a reduction in the local Nusselt number. Similarly, an increase in ϕ_2 when

(γ = 0.1 and ϕ_1 = 0.1), results in a contraction of the heat transfer rate. Conspicuously, the hybrid nanofluid with the least alumina concentration (ϕ_1 = 0.03 and ϕ_2 = 0.02) demonstrates a higher heat transfer rate than the one with higher alumina concentration (ϕ_1 = 0.1 and ϕ_2 = 0.02).

In exploring the intricate realm of hybrid nanofluids, this investigation elucidates the paradoxical relationship between their intended role in enhancing heat transfer and the observed reduction in the Nusselt number. The results unveiled a nuanced scenario wherein the addition of alumina under specific conditions (γ = 0.1 and ϕ_2 = 0.02), led to a counterintuitive decrease in the heat transfer rate. As nanoparticles volume fraction for alumina increased, a consequential rise in the skin friction coefficient occurred, causing a localized reduction in the Nusselt number. To provide a theoretical foundation for this discrepancy, insights from Myers *et al*. [28] were incorporated, emphasizing the non-Newtonian behaviour of nanofluids at volume fractions between 10% and 30%, as demonstrated through Buongiorno's model. This discrepancy challenges the conventional assumption that an increase in the Nusselt number uniformly signifies enhanced heat transfer, emphasizing the need to consider variations in nanoparticle concentration. Additionally, [29] introduced a rescaling approach that simplifies the evaluation of flow and physical parameters, particularly in nanofluids exhibiting non-Newtonian behaviour post 5–6% volumetric concentration of nanoparticles. This rescaling technique, shedding light on the complexities inherent in high volume fractions and providing a foundation for advancing understanding of nanofluid dynamics and heat transfer mechanisms. Since the higher composition of the nanoparticles measured in this study is 10%, we believe this value will affect the overall hybrid nanofluid.

4. Conclusion

An analysis was conducted on the flow of hybrid nanofluid past a permeable shrinking cylinder under the influence of a magnetic field. The transformed ODEs were efficiently solved using the shooting method coupled with the RKF45 technique in Maple software. Validation of the precision of these numerical solutions was achieved by comparing them with the findings obtained by [22], revealing a commendable level of agreement.
The study addresses the research questions outlined in the introduction, leading to the following key conclusions:

- Hybrid nanofluid with the least alumina volumetric concentration exhibits a higher heat transfer rate than the overall hybrid nanofluid.
- The addition of alumina and copper volumetric concentration contributes to a reduction in the heat transfer rate.
- The temperature profile experiences an increase with an enhancement of the curvature parameter and Eckert number, while it decreases with an increase in the magnetic parameter.
- The velocity profile only shows escalation with an increase in the magnetic parameter.

Acknowledgement

The authors would thank the Faculty of Applied Sciences and Technology, Universiti Tun Hussein Onn Malaysia for its support.

Conflict of Interest

Authors declare that there is no conflict of interests regarding the publication of the paper.

Author Contribution

The authors confirm contribution to the paper as follows: ***study conception and design:*** *Nur Syazwani Mat Yusof;* ***solve the governing equations:*** *Nur Syazwani Mat Yusof;* ***analysis and interpretation of results:*** *Nur Syazwani Mat Yusof, Fazlina Aman;* ***draft manuscript preparation:*** *Nur Syazwani Mat Yusof, Fazlina Aman. All authors reviewed the results and approved the final version of the manuscript.*

References

[1] Choi, S U.S., and Eastman, J A. (1995). Enhancing thermal conductivity of fluids with nanoparticles. *International mechanical engineering congress and exhibition*, San Francisco, C.A. https://www.osti.gov/servlets/purl/196525

[2] Jana, S., Salehi-Khojin, A., & Zhong, W.-H. (2007). Enhancement of fluid thermal conductivity by the addition of single and hybrid nano-additives. *Thermochimica Acta*, *462*(1–2), 45–55. https://doi.org/10.1016/j.tca.2007.06.009

[3] Wahab, A., Hassan, A., Qasim, M. A., Ali, H. M., Babar, H., & Sajid, M. U. (2019). Solar Energy Systems – potential of nanofluids. *Journal of Molecular Liquids*, *289*, 111049. https://doi.org/10.1016/j.molliq.2019.111049
[4] Mahanthesh, B., Animasaun, I. L., Rahimi-Gorji, M., & Alarifi, I. M. (2019). Quadratic convective transport of Dusty Casson and Dusty Carreau fluids past a stretched surface with nonlinear thermal radiation, convective condition and non-uniform heat source/sink. *Physica A: Statistical Mechanics and Its Applications*, *535*, 122471. https://doi.org/10.1016/j.physa.2019.122471
[5] Suresh, S., Venkitaraj, K. P., Selvakumar, P., & Chandrasekar, M. (2011). Synthesis of al2o3–cu/water hybrid nanofluids using two step method and its thermo physical properties. *Colloids and Surfaces A: Physicochemical and Engineering Aspects*, *388*(1–3), pp. 41–48. https://doi.org/10.1016/j.colsurfa.2011.08.005
[6] Awan, A. U., Ali, B., Shah, S. A., Oreijah, M., Guedri, K., & Eldin, S. M. (2023). Numerical Analysis of heat transfer in Ellis hybrid nanofluid flow subject to a stretching cylinder. *Case Studies in Thermal Engineering*, *49*, 103222. https://doi.org/10.1016/j.csite.2023.103222
[7] Wang, C. Y. (1988). Fluid flow due to a stretching cylinder. *The Physics of Fluids*, *31*(3), 466–468. https://doi.org/10.1063/1.866827
[8] Ishak, A., Nazar, R., & Pop, I. (2008). Uniform suction/blowing effect on flow and heat transfer due to a stretching cylinder. *Applied Mathematical Modelling*, *32*(10), 2059–2066. https://doi.org/10.1016/j.apm.2007.06.036
[9] Wang, C. Y., & Ng, C.-O. (2011). Slip flow due to a stretching cylinder. *International Journal of Non-Linear Mechanics*, *46*(9), 1191–1194. https://doi.org/10.1016/j.ijnonlinmec.2011.05.014
[10] Makhdoum, B. M., Mahmood, Z., Khan, U., Fadhl, B. M., Khan, I., & Eldin, S. M. (2023). Impact of suction with nanoparticles aggregation and Joule Heating on unsteady MHD stagnation point flow of nanofluids over horizontal cylinder. *Heliyon*, *9*(4). https://doi.org/10.1016/j.heliyon.2023.e15012
[11] Morrison, D. D., Riley, J. D., & Zancanaro, J. F. (1962). Multiple shooting method for two-point boundary value problems. *Communications of the ACM*, *5*(12), 613–614. https://doi.org/10.1145/355580.369128
[12] Keller, H. B. (1976). *Numerical Solution of Two Point Boundary Value Problems*. https://archive.org/details/numericalmethods00kell/page/n5/mode/2up
[13] Muhammad, K., Abdelmohsen, S. A. M., Abdelbacki, A. M. M., & Ahmed, B. (2022). Darcy-Forchheimer flow of hybrid nanofluid subject to melting heat: A comparative numerical study via shooting method. *International Communications in Heat and Mass Transfer*, *135*, 106160. https://doi.org/10.1016/j.icheatmasstransfer.2022.106160
[14] Li, S., Ijaz Khan, M., Rafiq, M., Abdelmohsen, S. A. M., Shukhratovich Abdullaev, S., & Amjad, M. S. (2023). Optimized framework for Darcy-Forchheimer flow with chemical reaction in the presence of Soret and Dufour Effects: A shooting technique. *Chemical Physics Letters*, *825*, 140578. https://doi.org/10.1016/j.cplett.2023.140578
[15] Daneshyar, A., & Ghaemian, M. (2021). A general solution procedure for the scaled boundary finite element method via shooting technique. *Computer Methods in Applied Mechanics and Engineering*, *384*, 113996. https://doi.org/10.1016/j.cma.2021.113996
[16] Selimefendigil, F., & Öztop, H. F. (2023). Forced convection of nanofluid in double vented cavity system separated by perforated conductive plate under magnetic field. *Engineering Analysis with Boundary Elements*, *149*, 18–26. https://doi.org/10.1016/j.enganabound.2023.01.004
[17] Kolsi, L., Selimefendigil, F., Omri, M., Rmili, H., Ayadi, B., Maatki, C., & Alshammari, B. M. (2023). CFD study of MHD and elastic wall effects on the nanofluid convection inside a ventilated cavity including perforated porous object. *Mathematics*, *11*(3), 695. https://doi.org/10.3390/math11030695
[18] Ouni, M., Selimefendigil, F., Hatem, B., Kolsi, L., & Omri, M. (2022). Utilization of wavy porous layer, magnetic field and hybrid nanofluid with slot jet impingement on the cooling performance of conductive panel. *International Journal of Numerical Methods for Heat & Fluid Flow*, *33*(1), 360–384. https://doi.org/10.1108/hff-03-2022-0192
[19] Selimefendigil, F., & Öztop, H. F. (2023). Combined effects of using multiple porous cylinders and inclined magnetic field on the performance of hybrid nanoliquid forced convection. *Journal of Magnetism and Magnetic Materials*, *565*, 170137. https://doi.org/10.1016/j.jmmm.2022.170137

[20] Selimefendigil, F., & Öztop, H. F. (2022). Hybrid nanofluid convection and phase change process in an expanded channel under the combined effects of double rotating cylinders and magnetic field. *Journal of Molecular Liquids*, *368*, 120364. https://doi.org/10.1016/j.molliq.2022.120364

[21] Xu, W., Huang, T., Huang, S.-M., & Zhuang, Y. (2023). Regulation mechanism of magnetic field on non-newtonian melting and energy storage performance of metal foam composite nano-enhanced phase change materials. *International Journal of Heat and Mass Transfer*, *200*, 123501. https://doi.org/10.1016/j.ijheatmasstransfer.2022.123501

[22] Khashi'ie, N. S., Arifin, N. M., Pop, I., & Wahid, N. S. (2020). Flow and heat transfer of hybrid nanofluid over a permeable shrinking cylinder with Joule Heating: A comparative analysis. *Alexandria Engineering Journal*, *59*(3), 1787–1798. https://doi.org/10.1016/j.aej.2020.04.048

[23] Tiwari, R. K., & Das, M. K. (2007). Heat transfer augmentation in a two-sided lid-driven differentially heated square cavity utilizing nanofluids. *International Journal of Heat and Mass Transfer*, *50*(9–10), 2002–2018. https://doi.org/10.1016/j.ijheatmasstransfer.2006.09.034

[24] Devi, S. P., & Devi, S. S. (2016). Numerical investigation of hydromagnetic hybrid Cu – Al2O3/water nanofluid flow over a permeable stretching sheet with suction. *International Journal of Nonlinear Sciences and Numerical Simulation*, *17*(5), 249–257. https://doi.org/10.1515/ijnsns-2016-0037

[25] Devi, S. U., & Devi, S. A. (2017). Heat transfer enhancement of Cu–Al_2O_3/water hybrid nanofluid flow over a stretching sheet. *Journal of the Nigerian Mathematical Society*, *36*(2), 419-433. https://www.semanticscholar.org/paper/Nigerian-Mathematical-Society-HEAT-TRANSFER-OF-Cu-%E2%88%92-Devi-Devi/5331616a8df2659325dcd43be41144fb26cfa9ed

[26] Devi, S. S., & Devi, S. P. A. (2016). Numerical investigation of three-dimensional hybrid Cu–Al2O3/water nanofluid flow over a stretching sheet with effecting Lorentz force subject to Newtonian heating. *Canadian Journal of Physics*, *94*(5), 490–496. https://doi.org/10.1139/cjp-2015-0799

[27] Oztop, H. F., & Abu-Nada, E. (2008). Numerical study of natural convection in partially heated rectangular enclosures filled with nanofluids. *International Journal of Heat and Fluid Flow*, *29*(5), 1326–1336. https://doi.org/10.1016/j.ijheatfluidflow.2008.04.009

[28] Myers, T. G., Ribera, H., & Cregan, V. (2017). Does mathematics contribute to the nanofluid debate? *International Journal of Heat and Mass Transfer*, *111*, 279–288. https://doi.org/10.1016/j.ijheatmasstransfer.2017.03.118

Turkyilmazoglu, M. (2015). A note on the correspondence between certain nanofluid flows and standard fluid flows. *Journal of Heat Transfer*, *137*(2). https://doi.org/10.1115/1.4028807